

**Revision 1<sup>st</sup> JULY 2020**

**Detection of perfluorooctane sulfonate by ion-transfer stripping voltammetry at an array of microinterfaces between two immiscible electrolyte solutions**

Benjamín N. Viada,<sup>1,2,3</sup> L. Mabel Yudi,<sup>2,3</sup> Damien W. M. Arrigan<sup>1\*</sup>

<sup>1</sup> *Curtin Institute for Functional Molecules and Interfaces, School of Molecular and Life Sciences, Curtin University, GPO Box U1987, Perth, Western Australia, 6845, Australia.*

<sup>2</sup> *Universidad Nacional de Córdoba, Facultad de Ciencias Químicas, Departamento de Fisicoquímica, Córdoba, Argentina.*

<sup>3</sup> *Consejo Nacional de Investigaciones Científicas y Técnicas CONICET, Instituto de Investigaciones en Fisicoquímica de Córdoba INFIQC, Córdoba, Argentina.*

## Abstract

Per- and polyfluoroalkyl substances (PFAS) are a category of persistent environmental contaminants that have been linked to health issues in humans. In this work, we investigate the detection of perfluorooctanesulfonate (PFOS<sup>-</sup>), one such PFAS, by ion-transfer voltammetry at an array of microinterfaces between two immiscible electrolyte solutions ( $\mu$ ITIES). Cyclic voltammetry, differential pulse voltammetry and differential pulse stripping voltammetry (DPSV) indicated the ion-transfer behaviour and detection of PFOS<sup>-</sup>, with the latter enabling detection at picomolar concentrations. Using a 5 min preconcentration time, during which PFOS<sup>-</sup> was preconcentrated into the organic phase of the  $\mu$ ITIES array, a limit of detection (LOD) of 0.03 nM (0.015  $\mu$ g/L) in aqueous electrolyte was achieved. This performance is attributed to the enhanced mass transport (radial diffusion) to the  $\mu$ ITIES that occurs during preconcentration. To investigate the potentiality for applications of this analytical approach to environmental samples, measurements in a range of water matrices were investigated. Drinking water, laboratory tap water and seawater matrices were assessed by spiking with PFOS<sup>-</sup> over the 0.1-1 nM range. A matrix effect was observed, with changes in sensitivity and LOD relative to those in pure aqueous electrolyte solutions. Such matrix effects need to be considered in designing applications of these PFOS<sup>-</sup> measurements to environmental samples. The results presented here indicate that DPSV at a  $\mu$ ITIES array can form the basis for a fast and sensitive screening method for PFOS<sup>-</sup> contamination that is suited to portable and on-site applications.

## 1. Introduction

Per- and polyfluoroalkyl substances (PFAS) have been widely used in industry due to their unique physicochemical and chemical properties. Their technological applications include in paper and packaging, as stain and water resistant coatings on carpet and clothing, as nonstick coatings on cookware, as industrial surfactants, in fire-resistant foams and in insecticide formulations.<sup>1,2</sup> However, their specific properties, such as stability, has led to the persistence of PFAS in the environment (soil, water), as well as in wildlife and humans.<sup>3,4,5,6,7,8</sup> This raises environmental and human health concerns due to the toxicity and bioaccumulation of PFAS. Taking into account this hazard, it is important to monitor the presence and concentrations of PFAS.<sup>9,10</sup> PFAS with long alkyl chains, such as perfluorooctanoate (PFOA) and perfluorooctanesulfonate (PFOS<sup>-</sup>), have been widely used, and as a result, these compounds represent the largest environmental and health concerns related with PFAS.<sup>11</sup>

Currently, several detection approaches are available for PFAS monitoring, including high-performance liquid chromatography–mass spectrometry (HPLC–MS), gas chromatography–mass spectrometry (GC–MS), liquid chromatography–tandem mass spectrometry (LC–MS–MS) and colourimetric detection.<sup>12,13,14,15,16,17,18</sup> Although excellent sensitivity has been achieved with these methods, they have disadvantages including economic costs, complex instrumentation, complicated sample pretreatment, and the need for highly trained personnel. They are also poorly suited to in-field measurements. There remains an on-going need for analytical approaches that allow PFAS detection at the required low concentrations in real matrices and that operate at short time with scope for in-field or in situ measurements. For example, minimum reporting levels for PFAS in drinking water have been set at the picomolar (nanogram per litre; parts per trillion) concentration range by the USA Environmental Protection Agency (EPA) and the Australian Department of Health.<sup>19,20</sup>

Although a wide range of electrochemical techniques have applied to determination of environmental pollutants,<sup>21, 22, 23, 24</sup> it is difficult to detect PFAS by direct redox electrochemistry because of the chemical stability of the carbon-fluorine bond. This problem might be resolved by employing electrochemistry at the interface between two immiscible electrolyte solutions (ITIES), which relies on the transfer of ionised species across the interface to generate the electrochemical signal. In other words, this approach can be used for analytical purposes without the need for analyte-based redox reactions. Several target analytes has been detected by ion transfer electrochemistry at the ITIES.<sup>25, 26, 27, 28</sup> However, traditional electrochemical cells

with a millimetre- or centimetre-scale interface are limited in their analytical usefulness due to linear diffusion and mechanical instability of the interface. These limitations can be overcome by miniaturization of the ITIES to microscale ( $\mu$ ITIES),<sup>29, 30, 31</sup> which enhances mass transport to the interface and improves the detection capabilities, while the mechanical stability can be improved by the use of a porous membrane to support the ITIES.<sup>32, 33</sup> There are a number of reports of the electrochemical characterisation and detection of pollutants,<sup>34</sup> proteins,<sup>35, 36, 37</sup> ionizable drugs,<sup>38, 39, 40</sup> macromolecules,<sup>41, 42</sup> and inorganic species<sup>43, 44</sup> at the  $\mu$ ITIES. Combination with differential pulse voltammetry (DPV) improved the LODs and the sensitivities compared to cyclic voltammetry (CV), due to discrimination against the capacitive current.<sup>45, 46</sup> Notably, the electrochemistry of some PFAS at the ITIES was investigated by Amemiya and co-workers,<sup>47</sup> in which ion-transfer electrochemistry was employed as a basis to measure their lipophilic properties, which may be a factor in the bioaccumulation and toxicity of these surfactants. Subsequently, this group also proposed a method for PFAS determination based on stripping voltammetry at the ITIES formed between an aqueous sample and a thin plasticized polymeric film supported on a gold disc electrode. Using a rotated electrode to improve mass transport to this ITIES and a preconcentration time of 30 min, they reported a LOD of 50 pM PFOS<sup>-</sup> ion in the presence of millimolar background electrolyte.<sup>26</sup> As an indication of interest in electrochemical approaches for PFOS<sup>-</sup> detection, recent papers reported its detection with LODs of 140 pM (using an electrochemical bubble nucleation method),<sup>48</sup> 40 pM (with a molecularly-imprinted polymer electrode)<sup>49</sup> and 1 pM (using a metal-organic framework impedimetric device).<sup>50</sup> Based on these antecedents, here we propose an electroanalytical approach for PFOS<sup>-</sup> employing a  $\mu$ ITIES array: by exploiting the enhanced (radial) diffusion at microinterfaces, the need for electrode rotation and long preconcentration times is removed, resulting in a simpler analytical strategy.<sup>51, 52</sup>

In this work, the voltammetric transfer and detection of perfluorooctanesulfonate (PFOS<sup>-</sup>), the most commonly-used PFAS, at an array of  $\mu$ ITIES formed between water and 1,2-dichloroethane (DCE) is reported. Investigations into combination of stripping and pulse voltammetric techniques (i.e. differential pulse stripping voltammetry (DPSV)) were undertaken. Preconcentration into the organic phase held within inverted truncated cone-shaped pores provided the capability for direct detection at environmentally-relevant concentrations. Based on this approach, it was possible to detect concentrations lower than the reporting levels for PFOS<sup>-</sup> in drinking water set by the USA EPA<sup>19</sup> and Australia's Department of Health.<sup>20</sup>

## 2. Experimental

### *Reagents*

All reagents were purchased from Sigma-Aldrich Australia, unless indicated otherwise. The electrolyte solutions were 10 mM LiCl (p.a. grade) in ultrapure water and 10 mM bis(triphenylphosphoranylidine)ammonium tetrakis (4-chlorophenylborate) (BTPPATPBCl) in 1,2-dichloroethane (DCE). BTPPATPBCl was prepared by metathesis of bis(triphenylphosphoranlidene)ammonium chloride (BTPPACl) and potassium tetrakis(4-chlorophenyl)borate (KTPBCl).

The surfactant perfluorooctanesulphonic acid (PFOS, purity: 97%) was purchased from Strem Chemicals Inc. (USA) and used as received. This compound was added to the aqueous phase of the electrochemical cell at different concentrations. At the natural pH of the 10 mM LiCl aqueous electrolyte solution (pH = 6), the surfactant was ionised and present in its anionic form, PFOS<sup>-</sup>. For studies of matrix effects on the electroanalytical signal, a range of natural and treated waters were examined, specifically drinking water (filtered, on-tap in Building 500 at Curtin University), laboratory tap water (not filtered for drinking purposes), and seawater (sampled from the Indian Ocean at Cottesloe Beach, Western Australia). These water samples were used, either as sampled or with added 10 mM LiCl, as the aqueous phase of the  $\mu$ ITIES array cell. In control experiments for the seawater matrix, the aqueous phase was artificial sea water (ASW), composed of sodium chloride (28.32 g/L), potassium chloride (0.77 g/L), magnesium chloride (5.48 g/L), magnesium sulfate (7.39 g/L) and calcium chloride (1.1 g/L).<sup>53</sup>

### *Electrochemical Measurements*

Cyclic voltammetry (CV), differential pulse voltammetry (DPV) and differential pulse stripping voltammetry (DPSV) were performed with an AUTOLAB PGSTAT302N potentiostat (Metrohm Autolab B.V., The Netherlands) controlled by NOVA software (version 2.1.2). Waveform parameters for DPV were as follows: step potential 5 mV, modulation amplitude 25 mV, modulation time 5 ms, interval time 0.5 s, scan rate 10

mVs<sup>-1</sup>; for DPSV, a preconcentration step at 0.1 V was implemented, for different times, as discussed below. Prior to each DPSV experiment, a preconditioning step of 0.5 V for 40 s was applied.

All experiments were performed using a glass membrane micropore array, consisting of 100 pores machined in 130 µm thick borosilicate glass substrates by laser ablation.<sup>43</sup> The fabrication process produced truncated cone-shaped pores, with a radius of 11.5 µm at the laser exit side of the membrane, and a radius of 26.5 µm at the laser entry side of the membrane. The laser exit side of the glass membrane and the internal pore walls were functionalized with trichloro-(1H,1H,2H,2H-perfluorooctyl)silane to make them hydrophobic, so that the organic phase filled the pores. In these experiments, the aqueous phase was placed on the membrane side with wider pore openings (laser entry side), and the organic phase was placed on the membrane side with the narrower pore openings (laser exit side), to favour analyte accumulation within the pores during stripping voltammetry experiments.<sup>54</sup> The glass membrane was glued to a glass tube with silicone sealant (Selley, Australia and New Zealand)<sup>55</sup> with the hydrophobic side facing the glass cylinder. The silicone was allowed to cure for 24 h and the assembly was subsequently rinsed with acetone/methanol and dried in air before electrochemical experiments. Then, the organic phase was placed into the glass tube and the organic reference solution was placed on top of the organic phase. The membrane and tube assembly was then inserted into the aqueous phase. Two Ag|AgCl reference electrodes completed the electrochemical cell, as depicted in Scheme 1.



Scheme 1. Electrochemical cell employed in investigating PFOS<sup>-</sup> detection at the µITIES array. The aqueous phase was 10 mM LiCl, a water sample matrix or artificial seawater, all spiked with PFOS<sup>-</sup> at different concentrations. The double vertical bar indicates the polarisable ITIES.

### 3. Results and discussion

**Voltammetric analysis at the  $\mu$ ITIES array.** The transfer of  $\text{PFOS}^-$  across the ITIES has been studied at micropipette-based ITIES by CV.<sup>56</sup> In that work, it was observed that this surfactant gave well-defined CVs with no voltammetric indication of adsorption, emulsification or instability of the interface. A sigmoidal voltammetric wave corresponding to transfer of the analyte from aqueous to organic phase coupled with nonlinear diffusion to the micrometer-sized interface was observed on the forward scan, and on the reverse scan, linear diffusion occurred when the transfer process was controlled by the species leaving the micropipette. Similar responses, but at  $\mu$ ITIES arrays, were observed in this work.

Figure 1 shows CVs employing a  $\mu$ ITIES array. The CV of the blank shows the background response, obtained when both phases contain only the background electrolyte species. The increased current at the negative end of the voltammogram is indicative of background electrolyte ion transfer across the ITIES. Moreover, when the aqueous phase contained 40  $\mu\text{M}$   $\text{PFOS}^-$  (Figure 1), an asymmetric CV was obtained with an apparent steady-state curve on the forward (negative-going) scan and a peak-shaped response on the reverse (positive-going) sweep. In comparison to Fig. S-1A, Fig. 1 indicates that  $\text{PFOS}^-$  does not have an ideal response at the  $\mu$ ITIES array. As was already reported for  $\text{PFOS}^-$ ,<sup>47</sup> it shows quasi-reversible ion-transfer behavior at the ITIES as confirmed by simulations for a simple, one step ion transfer process. Nevertheless, the differences between CVs in the presence and absence of  $\text{PFOS}^-$  (Fig. 1) indicate that this surfactant can be easily detected by voltammetry at the  $\mu$ ITIES array. For comparative purposes, CVs for perchlorate and perfluorooctanoate ( $\text{PFOA}^-$ ) were recorded in order to corroborate the response of this system with anions (Figure S-1, supporting information). Nevertheless, given the well-known limitations of CV for the detection of low concentrations of analytes, more sensitive voltammetric techniques are needed to achieve concentrations that are required for environmental monitoring.

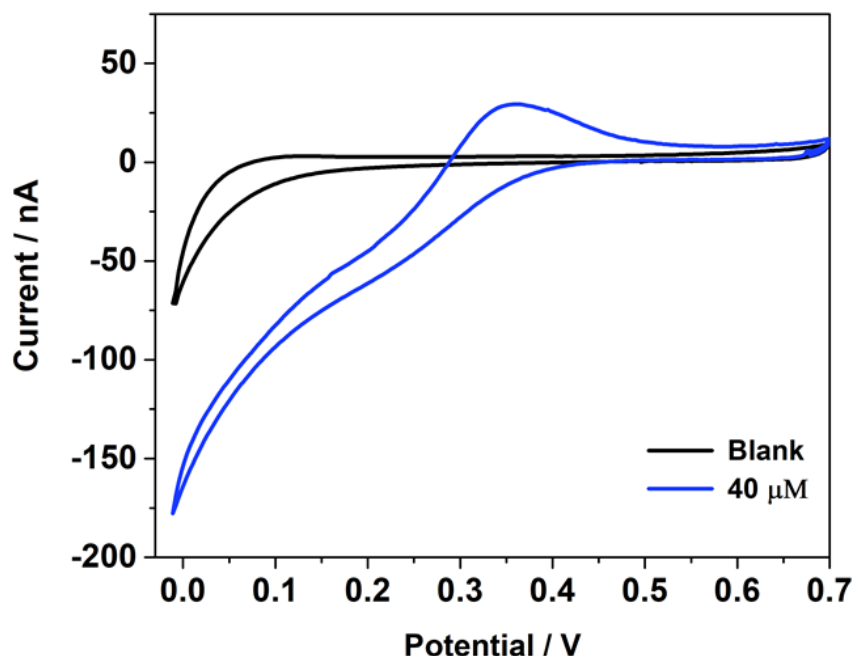


**Figure 1.** Cyclic voltammograms in the absence or presence of PFOS<sup>-</sup> transfer at the water | 1,2-dichloroethane micro-interface array. Aqueous phase composition: 10 mM LiCl + 40 μM PFOS<sup>-</sup> as indicated. Organic phase composition: 10 mM BTPPATPBCl.  $v = 0.010 \text{ V s}^{-1}$ .

**Differential pulse voltammetry at the μITIES array.** Although CV is capable of detecting PFOS<sup>-</sup>, DPV is generally employed to obtain an improved detection limit and sensitivity,<sup>56</sup> as already applied for the detection of ionized organic molecules at μITIES arrays.<sup>57,58</sup> Figure 2 shows background-subtracted DPVs for PFOS<sup>-</sup> at different concentrations, either in forward-direction scans (Fig. 2A) or reverse-direction scans (Fig. 2B). (Fig. S2 shows the DPV scans for the different concentrations of PFOS<sup>-</sup> and the blank scans used to prepare the background-subtracted DPVs). As for CV, forward or reverse scan directions correspond to PFOS<sup>-</sup> ion transfer from aqueous phase to organic phase or vice versa, respectively. As can be seen (Fig. 2), the PFOS<sup>-</sup> in the concentration range 0.1-1.0 μM were detected in both scan directions. The peak currents increased linearly with the concentration of PFOS<sup>-</sup> in this range, yielding LODs ( $3\sigma/m$ ) of 0.06 μM and 0.07 μM, for forward and reverse scan directions, respectively, and sensitivities (calibration line slopes) of 0.7 nA/μM and 0.8 nA/μM for forward and reverse scans, respectively. Thus, similar analytical figures of merit were possible by using a forward scan or a reverse scan, indicating that any preconcentration of PFOS<sup>-</sup> into the organic phase upon application of the initial potential for the reverse scan DPV, at which potential immediate PFOS<sup>-</sup> transfer into the organic phase occurs, was insufficient to provide a detection enhancement. Although DPV

was able to detect nanomolar concentrations, lower concentrations were not attempted with this method. Instead, it is important to note that an improvement in the LOD could be achieved by application of a systematic preconcentration step, so as to enable detection at or below the drinking water limits established by the USA EPA (0.04  $\mu\text{g/L}$ ; 80 pM)<sup>19</sup> and the Australian Department of Health (0.07  $\mu\text{g/L}$ ; 140 pM).<sup>20</sup> This approach, called stripping voltammetry, constitutes a powerful tool in electroanalytical strategies due to its high sensitivity.<sup>46,47</sup>

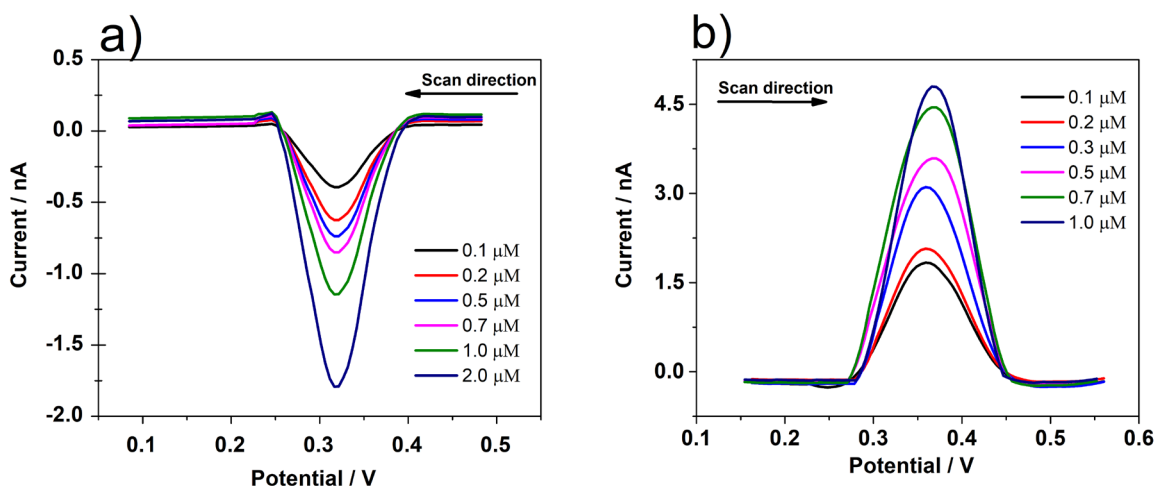


**Figure 2.** Differential pulse voltammetry (DPV) of increasing PFOS<sup>-</sup> concentrations at the  $\mu\text{ITIES}$  array for forward scan (a) and reverse scan (b). DPVs are background-subtracted. PFOS<sup>-</sup> concentrations: 0.1, 0.2, 0.3, 0.5, 0.7, 1  $\mu\text{M}$  (black) in the aqueous phase (10 mM LiCl). Organic phase composition: 10 mM BTTPATPBCl.

**Differential pulse stripping voltammetry at the  $\mu\text{ITIES}$  Array.** Improved detection of PFOS<sup>-</sup> was achieved by combination of stripping and pulse voltammetric techniques (i.e. differential pulse stripping voltammetry (DPSV)). This technique consisted of a preconcentration step at a fixed potential and a subsequent voltammetric detection step. The selection of the potential is crucial in DPSV because it is this factor which enables the preconcentration of the analyte into the organic phase so that the local concentration is elevated prior to detection in the subsequent stripping voltammetric step. This leads to lower LODs. Here, the potential selected for the preconcentration step was 0.1 V, based on the CV for PFOS<sup>-</sup> at the  $\mu\text{ITIES}$  array (Fig. 1). At this potential, the transfer of PFOS<sup>-</sup> from the aqueous to the organic phase occurs, increasing the concentration of this compound in the organic phase. Furthermore, the design of the micropores selected to support the  $\mu\text{ITIES}$  array, namely an inverted truncated cone, serves to keep the transferred analyte in the

organic phase within the pores, due to the sloped pore walls slowing down diffusion from the pores into the bulk organic phase.<sup>43,55</sup> After the preconcentration step, the analyte was stripped back into the aqueous phase using DPV (voltammetric step) by scanning from the preconcentration potential to higher potentials. Following selection of the applied potential, the influence of the preconcentration time on the DPSV response was investigated.

**Time dependence.** Figure 3 shows the results for DPSV of 10 nM PFOS<sup>-</sup> following preconcentration times in the range between 0.5 and 30 minutes; the inset shows the dependence of the stripping peak current on the preconcentration time (replicated data are shown in Fig. S3). As can be seen, the stripping peak current increased with the preconcentration time, but the rate is lower after 20 minutes, indicating a saturation effect. This type of saturation behavior was also observed for the stripping voltammetric detection of choline<sup>57</sup> oligopeptides<sup>58</sup>, drugs<sup>44</sup> and proteins<sup>35,58</sup>. Based on the results in Fig. 3, selection of the preconcentration time is a compromise between the peak current response and the time required for the analysis. In this case, one possible explanation for the saturation effect is that longer times result in a higher concentration of PFOS<sup>-</sup> in the organic phase, which might lead to formation of micellar aggregates (e.g. micelles, hemi-micelles)<sup>59</sup>. This could explain the loss of linearity with time (Fig. 3, inset), since an increase in surfactant concentration is not reflected in an increase in current because of PFOS<sup>-</sup> aggregation. Such behaviour has been reported for PFOS<sup>-</sup><sup>60</sup> and other PFAS.<sup>25</sup> Considering that the analyte transferred to the organic phase is solvated in DCE, the critical micelle concentration (CMC) will be different from that in water. However, although formation of PFAS reverse micelles in organic phases has been discussed,<sup>61</sup> no CMC values were reported. Nevertheless, it can be surmised that reverse micelles of PFOS<sup>-</sup> might form in the organic phase during the preconcentration step, and lead to the observed non-linear behaviour (Fig. 3).

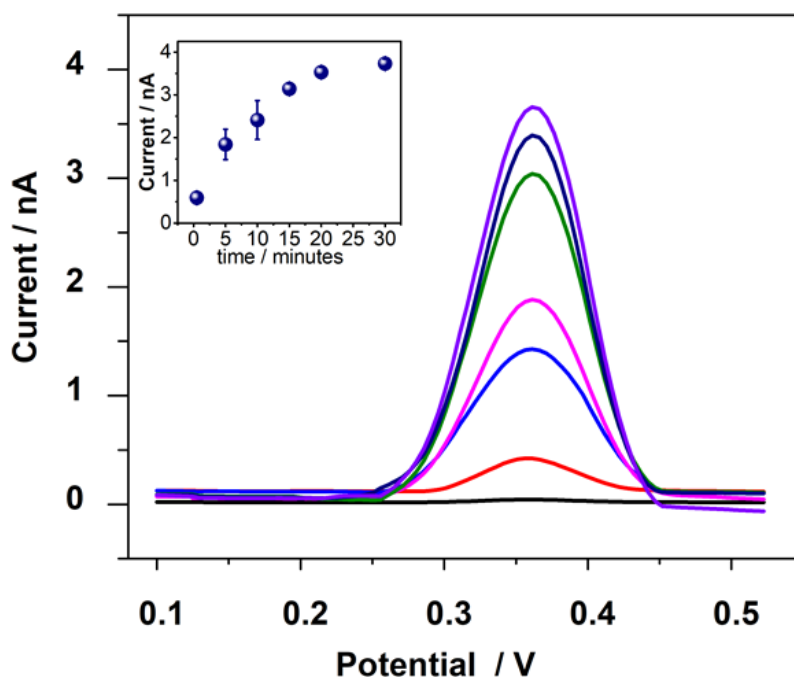


**Figure 3.** Influence of the preconcentration time on the DPSV (background-subtracted) of 10 nM PFOS<sup>-</sup> at the  $\mu$ ITIES array. Preconcentration times: 0.0, 0.5, 5, 10, 15, 20, 30 min. Inset: plot of stripping peak current versus preconcentration time, noting that the data point for 0.0 min preconcentration time is not shown in the inset graph. Data points are averages of three measurements and error bars are  $\pm 1$  standard deviation. Where error bars are not visible, they are smaller than the symbol size.

From an analytical perspective, longer times (10-15 min) yield larger stripping peak currents, but such time might be impractical from the point of view of a rapid analytical approach for applications in the field. Accordingly, in order to keep a short time for the analysis, 5 min was selected for the preconcentration time, as it provides a good signal intensity with a relatively short time. All subsequent experiments employed a preconcentration time of 5 min.

**Concentration range for PFOS<sup>-</sup> detection by DPSV.** DPSV responses to PFOS<sup>-</sup> were measured after 5 min preconcentration from unstirred solutions in the concentration range of 0.1-1.0 nM. The background-subtracted stripping voltammograms (Fig. 4) show clear stripping peaks that increase with PFOS<sup>-</sup> concentration (replicated data are shown in Fig. S4). There was a linear relationship between the peak current and the concentration in the studied concentration range (0.1-1.0 nM), (equation of straightline  $I_p = 1.73$

(nA/nM)(concentration) - 0.01 (nA),  $R^2 = 0.9964$ ,  $n = 10$ ). Remarkably, the LOD was 0.03 nM (0.015  $\mu\text{g/L}$ ). This value is at a similar picomolar level as reported using ion transfer stripping voltammetry at an aqueous-membrane interface supported on a modified gold electrode<sup>26</sup> and is  $\sim 1$  order of magnitude lower than reported for potentiometry at a fluoruous membrane electrode.<sup>23</sup> In the aqueous-membrane interface supported on a modified gold working electrode, the preconcentration time was 30 min and the electrode was rotated to enhance the mass transport of analyte to the interface. In contrast, in the present work, the preconcentration time was 5 min without rotation or stirring, presenting an important practical advantage. The relatively short preconcentration time was attributed to the increased mass-transport flux arising from radial diffusion at the  $\mu\text{ITIES}$  array.<sup>29-32, 43, 54, 55</sup> Additionally, DPV minimizes the contribution of the non-faradaic current to the differential current output, leading to the ability to detect lower concentrations of analyte.<sup>51,57</sup> On the other hand, conventional chromatographic methods including HPLC-MS, GC-MS and LC-MS-MS can achieve LODs of  $\sim 30$  ng/L (similar magnitude as presented here),<sup>62,63,64</sup> but these established methods require expensive and complex instruments and are often unsuitable for applications outside the laboratory. Taking into account these inconveniences, the detection of PFOS<sup>-</sup> using DPSV at a  $\mu\text{ITIES}$  array at picomolar concentrations opens up an interesting alternative to the established methods.

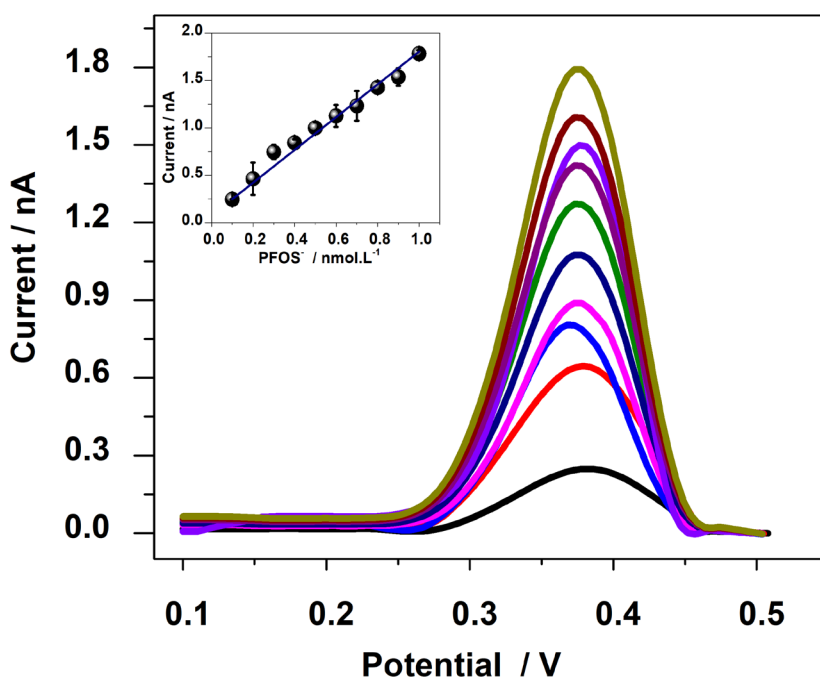


**Figure 4.** Electrochemistry of increasing concentrations of PFOS<sup>-</sup> at the  $\mu$ ITIES array using DPSV (background subtracted). Concentration range 0.1 to 1.0 nM PFOS<sup>-</sup>. Inset: calibration curve of current versus concentration. Data points are averages of three measurements and error bars are  $\pm 1$  standard deviation. Where error bars are not visible, they are smaller than the symbol size.

**Assessment of matrix effects.** In order to examine the possibility to apply ion-transfer DPSV to environmental analysis, its performance in a range of water samples was assessed. Laboratory tap water, drinking water and seawater were selected to assess the possible applicability of this analytical approach. These liquids were collected from the local water supply network at Curtin University, Perth, Australia or from the Indian Ocean on the coast of Perth, Australia. Before experiments, LiCl (10 mM) was added to all samples, in order to serve as a background electrolyte and to reduce any ohmic drop in the aqueous phase.<sup>65</sup> For these experiments, the stock solution of PFOS<sup>-</sup> used in spiking experiments was also prepared in the same water matrix; i.e. three different PFOS<sup>-</sup> stock solutions were prepared, depending on whether laboratory tap water, drinking water or seawater was being studied. This series of experiments was carried out with the objective of evaluating matrix effects on the analytical approach, specifically whether the sample matrix has an impact on the analytical performance. Matrix effects often cause the alteration of the analytical signal of target analytes in the presence of substances present in samples,<sup>66</sup> and can affect parameters of the measurements to cause erroneous quantification via either a decrease or an increase in the response.<sup>67</sup> The

first case is observed when there are interactions between the analyte and other components of the sample that may cause the detection of the analyte at a different potential than observed in standard solutions. On the other hand, an increase in response might occur when a component of the sample is detected at the same potential as the target analyte and results in a larger current. Both effects can alter analytical performance and, as a result, matrix effects must be characterised in order to evaluate the applicability of the proposed approach. To assess if substances commonly present in these waters, such as natural organic matter, interfere with the response, spiking with PFOS<sup>-</sup> was performed. Increasing concentrations of PFOS<sup>-</sup> were added to the three water types, from 0.1 nM to 1.0 nM. Figure 5 shows the results of the DPSV experiments.

For all three water types, the peak current increased with PFOS<sup>-</sup> concentration over the studied range. Nevertheless, changes in response in terms of the transfer potential observed or the magnitude of the current were observed. The transfer potential of PFOS<sup>-</sup> was altered in these matrices relative to the response in simple electrolyte solutions. This is attributed to the presence of different ions in these waters that can alter the Ag/AgCl reference electrode potential. These reference electrodes are dependent on the Cl<sup>-</sup> concentration in the solution; any shift in the reference electrode potential will cause an apparent shift in the observed analyte transfer potential. Additionally the presence of different ions can also affect the transfer of PFOS<sup>-</sup> directly, as will be discussed later. On the other hand, all water types showed a lower maximum current compared to the experiments conducted in electrolyte solutions prepared from ultrapure water. This signal decrease is attributed to the interaction of PFOS<sup>-</sup> with components of the matrix. For example, adsorption of the spiked PFOS<sup>-</sup> to the surfaces of any particulate matter<sup>67</sup> in the waters would result in a drop in the peak current, since the adsorbed compound is not available for transfer across the ITIES, or it transfers at a different applied potential. Adsorption of PFOS<sup>-</sup> onto surfaces of materials such as sand, clay, and minerals is a major factor in the fate and transport of these compounds in the environment.<sup>68,69</sup> One possible solution to this problem is the filtration of samples prior to electrochemical analysis, although this could result in removal of PFOS<sup>-</sup> from the samples, causing a false negative result. Note that in the seawater sample, there is an increase in current at potential above 0.4 V (Fig. 5c) that appears to be PFOS<sup>-</sup> dependent.

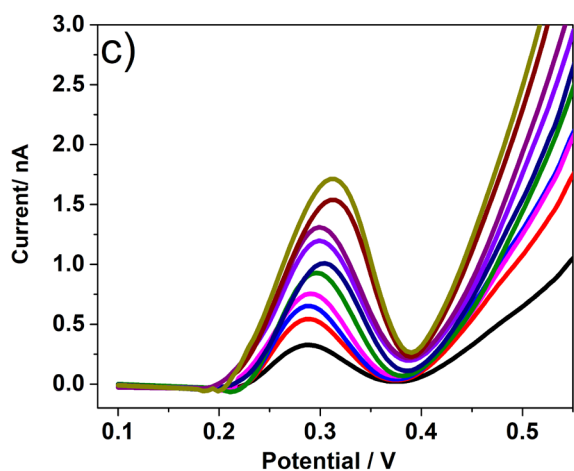
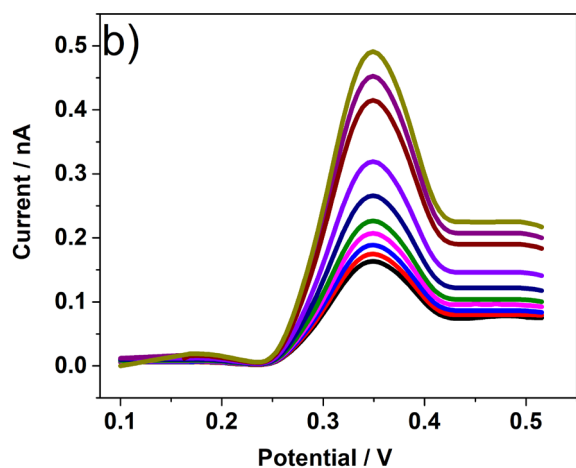
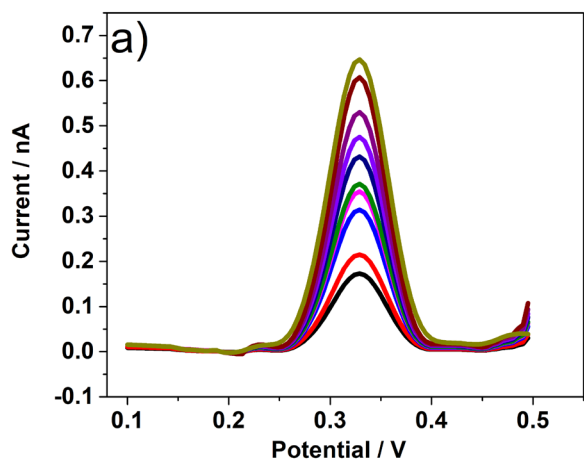


**Figure 5.** DPSV (background subtracted) at the  $\mu$ TIES array where the aqueous phase is different water sample matrices. Response from 0.1 to 1.0 nM PFOS<sup>-</sup>: a) for drinking water, b) for laboratory tap water, c) for seawater. Note that all water matrices also contained 10 mM LiCl.

In addition to water matrices fortified with LiCl (10 mM), measurements were also undertaken in drinking water and seawater without added supporting electrolyte (Figure 6). This constitutes an operational advantage since if the addition of supporting electrolytes is not necessary, samples may be measured directly. This approach is based on taking advantage of the ions naturally present in the samples to provide adequate supporting electrolytes as well as taking advantage of the ability of the  $\mu$ TIES to minimise the Ohmic drop in the electrochemical cell.<sup>70</sup> As seen in Fig. 6, the peak current increases with PFOS<sup>-</sup> concentration over the studied range but the maximum current was lower when compared to the same matrices with supporting electrolyte (Fig. 5a,c). It is important to note that for all the matrices, peak potential is around 0.3 – 0.35 V with small differences between them, except for the samples without LiCl (Fig. 6) where the peak potential is around 0.25 V (i.e. there is a shift towards lower potentials in the absence of LiCl). This could be an effect related with the presence of Li<sup>+</sup>, as this cation can interact with the charged group of PFOS<sup>-</sup> changing its hydrophilicity.<sup>71</sup> As a result, there causes a shift in the transfer potential of the analyte to more negatives values in the absence of added lithium cations. Nevertheless, more studies are needed to obtain a better understanding about the shift in the transfer potential of PFOS<sup>-</sup> when LiCl is present in solution. In order to perform a more rigorous comparison of the matrix effects, several analytical characteristics were determined.

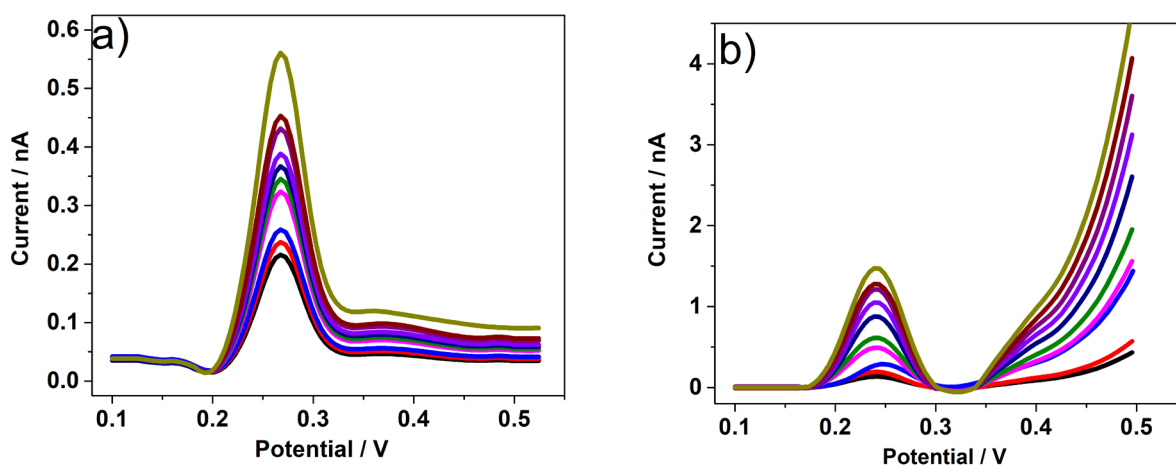


**Figure 6.** DPSV (background subtracted) at the  $\mu$ TIES array in different sample matrices without additional electrolyte. Response from 0.1 to 1.0 nM PFOS<sup>-</sup> a) for drinking water, b) for seawater.

**Analytical performance.** Table 1 summarises the analytical characteristics for PFOS<sup>-</sup> detection using ion-transfer DPSV in all matrices studied (see Figure S3, supporting information, for the calibration plots). As can be seen, the pure aqueous electrolyte (electrolyte solution prepared in ultrapure water) provided the greatest calibration graph slope (sensitivity) and the lowest calculated LOD (based on  $3\sigma/m$ ). For the real water matrices, the detection signal was attenuated and this is reflected in the analytical characteristics for these experiments (slope, LOD, etc). Surprisingly, the slope and LOD for the seawater was better than these parameters for laboratory tap water and drinking water. This unexpected result could be explained by the high concentration of ions in seawater. These ions interact with PFOS<sup>-</sup> and decrease its adsorption onto any particulate matter present. In this way, the PFOS<sup>-</sup> detection signal in the seawater matrix was not as affected as in the other matrices. There are several reports of this effect,<sup>67,72</sup> which concluded that the adsorption of PFOS<sup>-</sup> decreased with an increase in ionic strength, due to compression of the electrical double layer. Based on this, the response to PFOS<sup>-</sup> in seawater is better than in drinking water and tap water, since the latter do not have sufficient ions to produce the afore mentioned effect. The switch from pure electrolyte solution to water matrices resulted in changes in slopes of the calibration graphs for all matrices (Table 1, Slope difference (%)). In the absence of a matrix effect, the slopes of the calibration curves constructed in different matrices would be the same as in the pure electrolyte solution. However, the differences in slopes indicate a matrix effect that alters the analytical performance for PFOS<sup>-</sup> detection. This indicates that it is necessary to implement a strategy to minimize the matrix effect in order to use ion-transfer stripping voltammetry for the detection of PFOS<sup>-</sup> in waters. Standard addition calibration is one such method to compensate the matrix effect.<sup>73</sup> Taking these observations into account, future studies will be targeted to minimize the matrix effect. For instance, increasing the preconcentration time will produce a greater signal relative to the background. Another approach is to use an extraction method to isolate the target analyte from the sample matrix prior to electrochemical measurement, as employed recently by Luo and colleagues,<sup>48</sup> who combined solid-phase extraction of PFAS<sup>-</sup> with a bubble nucleation electrochemical detection method.

**Table 1.** Analytical performance for PFOS<sup>-</sup> in purified water and different water sample matrices.

	<i>Calibration graph Slope<sup>a</sup> / nA.nM<sup>-1</sup></i>	<i>Calibration graph Intercept<sup>a</sup> / nA</i>	<i>Concentration range studied / nM</i>	<i>Limit of detection (LOD)<sup>b</sup> / nM</i>	<i>R<sup>2</sup></i>	<i>% Slope difference</i>
<b>Ultrapure Water</b>	1.73 ± 0.04	-0.01 ± 0.02	0.1 – 1.0	0.03	0.99	100
<b>Drinking water</b>	0.48 ± 0.02	0.09 ± 0.01	0.1 – 1.0	0.09	0.99	28
<b>Tap Water</b>	0.43 ± 0.03	0.04 ± 0.02	0.1 – 1.0	0.14	0.97	25
<b>Sea Water</b>	0.95 ± 0.04	0.02 ± 0.02	0.1 – 1.0	0.06	0.98	55
<b>Drinking water (without LiCl)</b>	0.35 ± 0.28	0.02 ± 0.04	0.1 – 1.0	0.30	0.99	20
<b>Sea water (without LiCl)</b>	0.82 ± 0.08	-0.03 ± 0.04	0.1 – 1.0	0.16	0.96	47
<b>Artificial sea water (ASW)</b>	1.06 ± 0.03	-0.04 ± 0.03	0.1 – 1.0	0.07	0.96	61

<sup>a</sup> values quoted are ±1 standard deviation. <sup>b</sup> LOD calculated from  $3.\sigma/m$ , where  $\sigma$  is standard deviation of the blank(intercept);  $m$  is the calibration graph slope.

The differences between the calibration slopes for laboratory tap water and drinking water were insignificant and suggest that the effect on the transfer of PFOS<sup>-</sup> is the same for both water types. This is expected, since the compositions of these waters are similar. Furthermore, for the drinking water and seawater measurements without added supporting electrolyte, the results were different for each sample type. As might be expected for seawater samples, the difference between the calibration slopes with and without added supporting electrolyte was lower than that observed for drinking water, due to the high ionic strength of the seawater.<sup>74</sup> In other words, the addition of supporting electrolyte to the seawater matrix produced small changes in the sensitivity for the detection of PFOS<sup>-</sup> using the approach investigated here, although there is a change in LOD, attributed to the magnitude of the standard deviation of the intercept (used in calculating the LOD). With respect to the drinking water matrix, there is a significant difference between the calibration slopes with and without added supporting electrolyte, as well as in the calculated LODs (which depend on the slope). This is because drinking water does not have sufficient concentration of ions<sup>75</sup> to swamp the addition of LiCl and the addition of supporting electrolyte is necessary in drinking water in order to achieve a better sensitivity. For all matrices studied, the LODs were greater than achieved in pure electrolyte solutions

and greater than the minimum reporting level set by the U.S.A. EPA (80 pM<sup>19</sup>), except for sea water and ASW matrices where the LODs were a little lower than the reference value. On the other hand, mostly lower than the level set by the Department of Health, Australia (140 pM<sup>20</sup>). Nevertheless, the LOD obtained for all samples using DPSV at the  $\mu$ ITIES array reinforces the above comment on the need to minimize the matrix effect in a manner that enables a better analytical performance for the detection of PFOS<sup>-</sup> in real water samples.

**PFOS<sup>-</sup> response in artificial seawater matrix.** Finally, as can be seen in Fig. 5C and Fig. 6B, there is an increase in current at potentials more positive than the transfer potential of PFOS<sup>-</sup> for measurements in the seawater matrix. In order to determine if any of the matrix components were responsible for this increase in current, PFOS<sup>-</sup> detection was performed in a synthetic matrix that mimics seawater, in a similar manner to previous studies that assessed performance in artificial urine<sup>76</sup> and saliva.<sup>45</sup> Initial experiments to characterize the influence of an artificial sea water (ASW) matrix on ion-transfer DPSV showed that the components present in this mixture decreased the available potential window relative to that achieved when the aqueous phase consisted of supporting electrolyte (LiCl, 10 mM). The transfer of ions present in the ASW matrix significantly reduced the potential window, therefore limiting the working range. Figure 7 shows the DPSV of PFOS<sup>-</sup> in the ASW matrix, and can be directly compared with the response in real seawater.

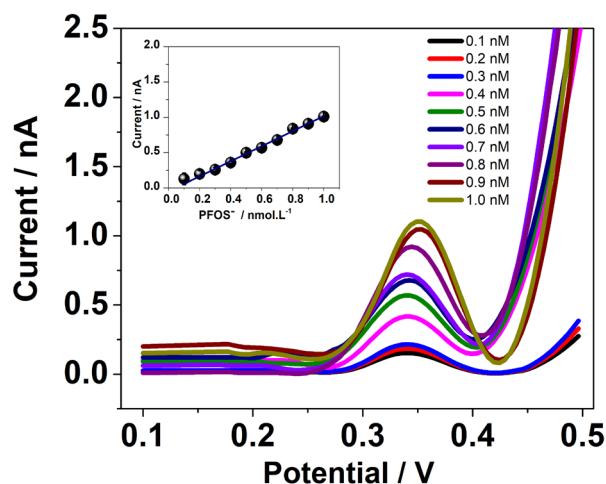


**Figure 7.** DPSV (background subtracted) of increasing concentrations of PFOS<sup>-</sup> in artificial seawater at the  $\mu$ ITIES array. Response from 0.1 to 1.0 nM PFOS<sup>-</sup>. Inset: calibration curve of current vs concentration. Data points are averages of three measurements and error bars are  $\pm 1$  standard deviation. Where error bars are not visible, they are smaller than the symbol size.

As can be seen, the background-subtracted stripping voltammograms show that the stripping peak currents increase with PFOS<sup>-</sup> concentration and a linear fit was obtained in the studied concentration range (0.1-1.0 nM). The equation of the linear fit was:  $I_p = 1.06 \text{ (nA/nM)}(\text{concentration}) - 0.04 \text{ (nA)}$ ,  $R^2 = 0.9964$ ,  $n = 10$ . The analytical characteristics calculated for the detection of PFOS in ASW are listed in Table 1. The sensitivity was lower compared to that in pure aqueous electrolyte due to the influence of the ASW matrix ions, as discussed above for the real seawater matrix. There are only slight differences in sensitivity (calibration graph slope) between the real seawater samples (with and without LiCl) and the ASW matrix (taking into consideration the magnitude of the respective standard deviations), indicating the importance of high ion concentration in the transfer of PFOS<sup>-</sup> in the studied system. Nevertheless the increase in current above 0.4 V is present in the ASW matrix as well as the seawater samples: this might be a feature of the high ion concentration and will require additional experiments to understand it.

## 4. Conclusions

In this work, it was demonstrated that PFOS<sup>-</sup>, an important environmental contaminant, can be detected by voltammetry at liquid-liquid interfaces supported on a microporous glass membrane. By combination of stripping and pulse voltammetric techniques (DPSV), an ultrasensitive analytical approach based on a constant-potential preconcentration step of five minutes, followed by a voltammetric detection step, was investigated. This approach enabled the detection of picomolar concentrations of PFOS<sup>-</sup> in aqueous solutions. A calculated LOD of 0.03 nM (0.015 µg/L) was obtained, which is lower than the reference levels for PFOS<sup>-</sup> in drinking water set by the U.S.A. EPA<sup>19</sup> and the Department of Health, Australia.<sup>20</sup> Furthermore, the impact of real sample matrices on the analytical performance was evaluated, and has shown that matrix components of the studied water types (laboratory tap water, drinking water and seawater) affect the analytical performance (sensitivities and LODs). Therefore, strategies to minimize the matrix effect for analysis of multiple samples, like standards addition calibration, are needed for practical applications of these findings. Finally, this work is based on electrochemical measurements at liquid-liquid interfaces, which can be implemented with any suitable electrochemical instrumentation. As a result, this work opens up a strategy to detecting PFOS<sup>-</sup> in the field with a fast and uncomplicated method implemented with portable instrumentation. In the future, this approach will enable the screening of samples or rapid on-site analysis, prior to further analysis of positive samples by conventional laboratory methods (e.g. HPLC–MS, GC-MS), considerably reducing the analysis time of a large number of samples. Finally, strategies to improve the detection limit to lower concentrations, e.g. by increasing the preconcentration time or altering the mass transport regime during the preconcentration step, mean that the results presented here provide a basis for further improvement in PFOS<sup>-</sup> detection in a simple and low-cost manner.

## Conflicts of interest

The authors declare no other conflicts of interest.

## Acknowledgements

Financial support from the Consejo Nacional de Investigaciones Científicas y Tecnológicas (CONICET), the Secretaría de Ciencia y Tecnología de la Universidad Nacional de Córdoba (SECyT - UNC) and the Agencia Nacional de Promoción Científica y Tecnológica (ANPCyT, FONCyT) are gratefully acknowledged. B.N.

Viada thanks CONICET for the award of fellowships and thanks the Curtin Institute for Functional Molecules and Interfaces for support of his visit to Curtin University.

## References

- 1 P. A. Fair, B. Wolf, N. D. White, S. A. Arnott, K. Kannan, R. Karthikraj and J. E. Vena, *Environ. Res.*, 2019, **171**, 266–277.
- 2 Y.-J. Jeong, S. Bang, J. Kim, S.-H. Chun, S. Choi, J. Kim, M.-S. Chung, G. J. Kang, Y.-W. Kang, J. Kim, Y. Kho, Y. Joo and K.-W. Lee, *Food Chem. Toxicol.*, 2019, **126**, 199–210.
- 3 Y. Liu, J. Su, R. M. van Dam, K. Prem, J. Y. S. Hoong, L. Zou, Y. Lu and C. N. Ong, *Chemosphere*, 2017, **171**, 617–624.
- 4 N. Hansmeier, T.-C. Chao, J.B. Herbstman, L.R. Goldman, F.R. Witter and R.U. Halden, *J. Proteome Res.*, 2015, **14**, 51-5.
- 5 N. Wu, D. Cai, M. Guo, M. Li and X. Li, *Sci. Total Environ.*, 2019, **667**, 594–600.
- 6 I. A. Rodríguez-Jorquera, R. C. Colli-Dula, K. Kroll, B. S. Jayasinghe, M. V. Parachu Marco, C. Silva-Sanchez, G. S. Toor and N. D. Denslow, *Environ. Sci. Technol.*, 2019, **53**, 1441–1452.
- 7 N. Briels, T. M. Ciesielski, D. Herzke and V. L. B. Jaspers, *Environ. Sci. Technol.*, 2018, **52**, 12859–12867.
- 8 B. Viada, C. I. Cámara and L. M. Yudi, *Soft Matter*, 2019, **15**, 2447–2462.
- 9 M. Houde, A. O. De Silva, D. C. G. Muir and R. J. Letcher, *Environ. Sci. Technol.*, 2011, **45**, 7962–7973.
- 10 M. Houde, J. W. Martin, R. J. Letcher, K. R. Solomon and D. C. G. Muir, *Environ. Sci. Technol.*, 2006, **40**, 3463–3473.
- 11 R. Mahinroosta and L. Senevirathna, *J. Environ. Manage.*, 2020, **255**, 109896.
- 12 T. Takayanagi, H. Yamashita, S. Motomizu, J. Musijowski and M. Trojanowicz, *Talanta*, 2008, **74**, 1224–1230.
- 13 M. Takino, S. Daishima and T. Nakahara, *Rapid Commun. Mass Spectrom. RCM*, 2003, **17**, 383–390.
- 14 P. Giusto, P. Lova, G. Manfredi, S. Gazzo, P. Srinivasan, S. Radice and D. Comoretto, *ACS Omega*, 2018, **3**, 7517–7522.
- 15 N. Cennamo, G. D'Agostino, F. Sequeira, F. Mattiello, G. Porto, A. Biasiolo, R. Nogueira, L. Bilro and L. Zeni, *Sensors*, 2018, **18**, 3009.
- 16 S. Poothong, S. K. Boontanon and N. Boontanon, *J. Hazard. Mater.*, 2012, **205–206**, 139–143.
- 17 M. Surma, M. Piskula, W. Wiczowski and H. Zieliński, *Eur. Food Res. Technol.*, 2017, **243**, 297–307.
- 18 C. Tang, J. Tan, C. Wang and X. Peng, *J. Chromatogr. A*, 2014, **1341**, 50–56.
- 19 Methods and Contaminants for the Unregulated Contaminant Monitoring Rule 3 (UCMR 3). UCMR 3 Contaminants and Corresponding Analytical Methods. Assessment Monitoring (List 1 Contaminants). <https://www.epa.gov/dwucmr/third-unregulated-contaminant-monitoring-rule> (accessed 07/April/2020)
- 20 Department of Health, Health Based Guidance Values for Per- and Poly-Fluoroalkyl Substances (PFAS), <https://www1.health.gov.au/internet/main/publishing.nsf/Content/ohp-pfas-hbgv.htm> (accessed 07/April/2020).
- 21 M. Liu, G. Zhao, Y. Tang, Z. Yu, Y. Lei, M. Li, Y. Zhang and D. Li, *Environ. Sci. Technol.*, 2010, **44**, 4241–4246.
- 22 G. Hernandez-Vargas, J. E. Sosa-Hernández, S. Saldarriaga-Hernandez, A. M. Villalba-Rodríguez, R. Parra-Saldivar and H. M. N. Iqbal, *Biosensors*, 2018, **8**, 29.
- 23 L. D. Chen, C.-Z. Lai, L. P. Granda, M. A. Fierke, D. Mandal, A. Stein, J. A. Gladysz and P. Bühlmann, *Anal. Chem.*, 2013, **85**, 7471–7477.
- 24 T. Tran, T. J. Li, H. Feng, J. Cai, L. Yuan, N. Wang and Q. Cai, *Sens. Actuat. B Chem.*, 2014, **190**, 745–751.
- 25 B. N. Viada, A. V. Juárez, E. M. Pachón Gómez, M. A. Fernández and L. M. Yudi, *Electrochim. Acta*,

- 2018, **263**, 499–507.
- 26 M. B. Garada, B. Kabagambe, Y. Kim and S. Amemiya, *Anal. Chem.*, 2014, **86**, 11230–11237.
- 27 T. Osakai, Y. Yuguchi, E. Gohara and H. Katano, *Langmuir*, 2010, **26**, 11530–11537.
- 28 G. Herzog, S. Flynn, C. Johnson and D. W. M. Arrigan, *Anal. Chem.*, 2012, **84**, 5693–5699.
- 29 D. W. M. Arrigan and G. Herzog, *Curr. Opin. Electrochem.*, 2017, **1**, 66–72.
- 30 G. Herzog, *Analyst*, 2015, **140**, 3888–3896.
- 31 G. Taylor and H. H. J. Girault, *J. Electroanal. Chem. Interfacial Electrochem.*, 1986, **208**, 179–183.
- 32 A. A. Stewart, G. Taylor, H. H. Girault and J. McAleer, *J. Electroanal. Chem. Interfacial Electrochem.*, 1990, **296**, 491–515.
- 33 Y. Liu, M. Sairi, G. Neusser, C. Kranz and D. W. M. Arrigan, *Anal. Chem.*, 2015, **87**, 5486–5490.
- 34 Md. M. Hossain, S. N. Faisal, C. S. Kim, H. J. Cha, S. C. Nam and H. J. Lee, *Electrochem. Commun.*, 2011, **13**, 611–614.
- 35 H. Sakae, Y. Toda and T. Yokoyama, *Electrochem. Commun.*, 2018, **90**, 83–86.
- 36 G. Herzog, P. Eichelmann-Daly and D. W. M. Arrigan, *Electrochem. Commun.*, 2010, **12**, 335–337.
- 37 D. W. M. Arrigan, M. J. Hackett and R. L. Mancera, *Curr. Opin. Electrochem.*, 2018, **12**, 27–32.
- 38 H. Sakae, M. Fujisawa, H. Nagatani and H. Imura, *J. Electroanal. Chem.*, 2016, **782**, 288–292.
- 39 H. Sakae, H. Nagatani and H. Imura, *Electrochim. Acta*, 2016, **191**, 631–639.
- 40 S. Jeshycka, H. Y. Han and H. J. Lee, *Electrochim. Acta*, 2017, **245**, 211–218.
- 41 B. M. B. Felisilda, A. D. Payne and D. W. M. Arrigan, *Anal. Chem.*, 2018, **90**, 10256–10262.
- 42 J. S. Riva, D. M. Beltramo and L. M. Yudi, *Electrochim. Acta*, 2014, **115**, 370–377.
- 43 E. Alvarez de Eulate, J. Strutwolf, Y. Liu, K. O'Donnell and D. W. M. Arrigan, *Anal. Chem.*, 2016, **88**, 2596–2604.
- 44 Md. M. Hossain, S. H. Lee, H. H. Girault, V. Devaud and H. J. Lee, *Electrochim. Acta*, 2012, **82**, 12–18.
- 45 C. J. Collins and D. W. M. Arrigan, *Anal. Chem.*, 2009, **81**, 2344–2349.
- 46 G. Herzog and V. Beni, *Anal. Chim. Acta*, 2013, **769**, 10–21.
- 47 P. Jing, P. J. Rodgers and S. Amemiya, *J. Am. Chem. Soc.*, 2009, **131**, 2290–2296
- 48 R. Ranaweera, C. Ghafari and L. Luo, *Anal. Chem.*, 2019, **91**, 7744–7748
- 49 N. Karimian, A. M. Stortini, L. M. Moretto, C. Costantino, S. Bogialli, and P. Ugo, *ACS Sens.*, 2018, **3**, 1291–1298.
- 50 Y. H. Cheng, D. Barpaga, J. A. Soltis, V. Shutthanandan, R. Kargupta, K. S. Han, B. P. McGrail, R. K. Motkuri, S. Basuray and S. Chatterjee, *ACS Appl. Mater. Interfaces*, 2020, **12**, 10503–10514.
- 51 J. Strutwolf, M. D. Scanlon and D. W. M. Arrigan, *J. Electroanal. Chem.*, 2010, **641**, 7–13.
- 52 D.W.M. Arrigan, G. Herzog, M.D. Scanlon, J. Strutwolf, in *Electroanalytical Chemistry, A Series of Advances*, edited by A.J. Bard & C.G. Zoski, 2013, vol. 25, 105–178, CRC Press, Boca Raton.
- 53 C. K. Sekhar, S. N. Chary, K. C. Tirumala and V. Aparna, *Acta Chim Slov*, 2003, **11**.
- 54 J. Strutwolf and D. W. M. Arrigan, *Anal. Bioanal. Chem.*, 2010, **398**, 1625–1631.
- 55 E. Alvarez de Eulate and D. W. M. Arrigan, *Anal. Chem.*, 2012, **84**, 2505–2511.
- 56 T. R. Brumleve and Janet. Osteryoung, *Anal. Chem.*, 1981, **53**, 988–991.
- 57 H. J. Lee, C. Beriet and H. H. Girault, *Anal. Sci.*, 1998, **14**, 71–77.
- 58 M. D. Scanlon, G. Herzog and D. W. M. Arrigan, *Anal. Chem.*, 2008, **80**, 5743–5749.
- 59 X. Wang, J. Chen, D. Wang, S. Dong, J. Hao and H. Hoffmann, *Adv. Colloid Interface Sci.*, 2017, **246**, 153–164.
- 60 J. H. Jun, K. Sawada and M. Ueda, *Dyes Pigments*, 2004, **61**, 17–22.
- 61 P. Meng, S. Deng, Z. Du, B. Wang, J. Huang, Y. Wang, G. Yu and B. Xing, *Sci. Rep.*, 2017, **7**, 44694.
- 62 C. Gremmel, T. Frömel and T. P. Knepper, *Anal. Bioanal. Chem.*, 2017, **409**, 1643–1655.
- 63 M. Trojanowicz and M. Koc, *Mikrochim. Acta*, 2013, **180**, 957–971.
- 64 C. A. Huset and K. M. Barry, *MethodsX*, 2018, **5**, 697–704.
- 65 M. Senda, T. Kakiuchi and T. Osaka, *Electrochim. Acta*, 1991, **36**, 253–262.
- 66 W. Zhou, S. Yang and P. G. Wang, *Bioanalysis*, 2017, **9**, 1839–1844.
- 67 F. Wang and K. Shih, *Water Res.*, 2011, **45**, 2925–2930.

- 68 R. L. Johnson, A. J. Anschutz, J. M. Smolen, M. Simcik and L. Penn, *J. Chem. Eng. Data*, 2007, **52**, 1165–1170.
- 69 Y. Yao, K. Volchek, C. E. Brown, A. Robinson and T. Obal, *Water Sci. Technol. J. Int. Assoc. Water Pollut. Res.*, 2014, **70**, 1983–1991.
- 70 J. S. Riva, V. C. Bassetto, H. H. Girault and A. J. Olaya, *J. Electroanal. Chem.*, 2019, **835**, 192–196.
- 71 C. F. Poole and S. K. Poole, *J. Chromatogr. A*, 1997, **792**, 89–104.
- 72 D. Q. Zhang, W. L. Zhang and Y. N. Liang, *Sci. Total Environ.*, 2019, **694**, 133606.
- 73 M. Gergov, T. Nenonen, I. Ojanpera and R. A. Ketola, *J. Anal. Toxicol.* 2015, **39**, 359–364.
- 74 F. J. Millero, S. Hubinger, M. Fernandez and S. Garnett, *Environ. Sci. Technol.*, 1987, **21**, 439–443.
- 75 Drinking Water Quality Perth & WA, Water Quality Testing & More, <https://www.watercorporation.com.au/about-us/our-performance/drinking-water-quality> (accessed 07/April/2020).
- 76 C. J. Collins, A. Berduque and D. W. M. Arrigan, *Anal. Chem.*, 2008, **80**, 8102–8108.

## Electronic Supplementary Information

### Detection of perfluorooctane sulfonate by ion-transfer stripping voltammetry at an array of microinterfaces between two immiscible electrolyte solutions

Benjamín N. Viada,<sup>1,2,3</sup> L. Mabel Yudi,<sup>2,3</sup> Damien W. M. Arrigan<sup>1\*</sup>

<sup>1</sup> Curtin Institute for Functional Molecules and Interfaces, School of Molecular and Life Sciences, Curtin University, GPO Box U1987, Perth, Western Australia, 6845, Australia.

<sup>2</sup> Universidad Nacional de Córdoba, Facultad de Ciencias Químicas, Departamento de Físicoquímica, Córdoba, Argentina.

<sup>3</sup> Consejo Nacional de Investigaciones Científicas y Técnicas CONICET, Instituto de Investigaciones en Físicoquímica de Córdoba INFIQC, Córdoba, Argentina.

**Summary.** This supporting information contains

- Figure S1. experimental CVs for perfluorooctanoate (PFOA) and  $\text{ClO}_4^-$ ;
- Figure S2. as-recorded DPVs for  $\text{PFOS}^-$ : at different concentrations and blank (background) scans.
- Figure S3. Background-subtracted DPSV for  $\text{PFOS}^-$  in electrolyte solution with different preconcentration times; two sets of data are replicates of the data shown in Figure 3;
- Figure S4. Background-subtracted DPSV for  $\text{PFOS}^-$  in electrolyte solution with different concentrations of  $\text{PFOS}^-$ ; the two sets of data are replicates of data shown in Figure 4;
- Figure S5. Calibration curve plots for  $\text{PFOS}^-$  spiked into various water matrices and detected by DPSV.

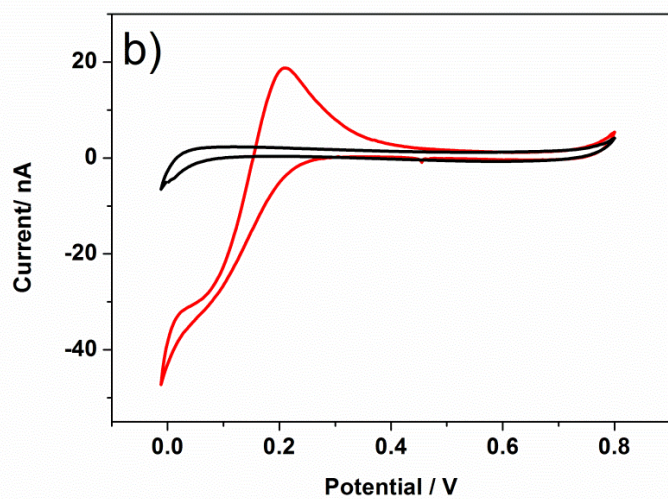
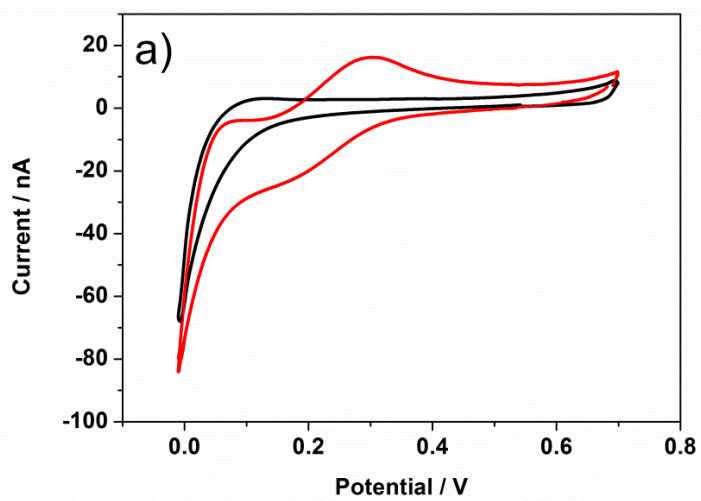


**Figure S1.** Cyclic voltammograms for PFOA 40  $\mu\text{M}$  (a) and  $\text{ClO}_4^-$  40  $\mu\text{M}$  (b) transfer at the water/1,2-dichloroethane micro-interface array. Aqueous phase composition: analyte + 10 mM LiCl. Organic phase composition: 10 mM BTPPATPBCl.  $\nu = 0.010 \text{ V s}^{-1}$ .

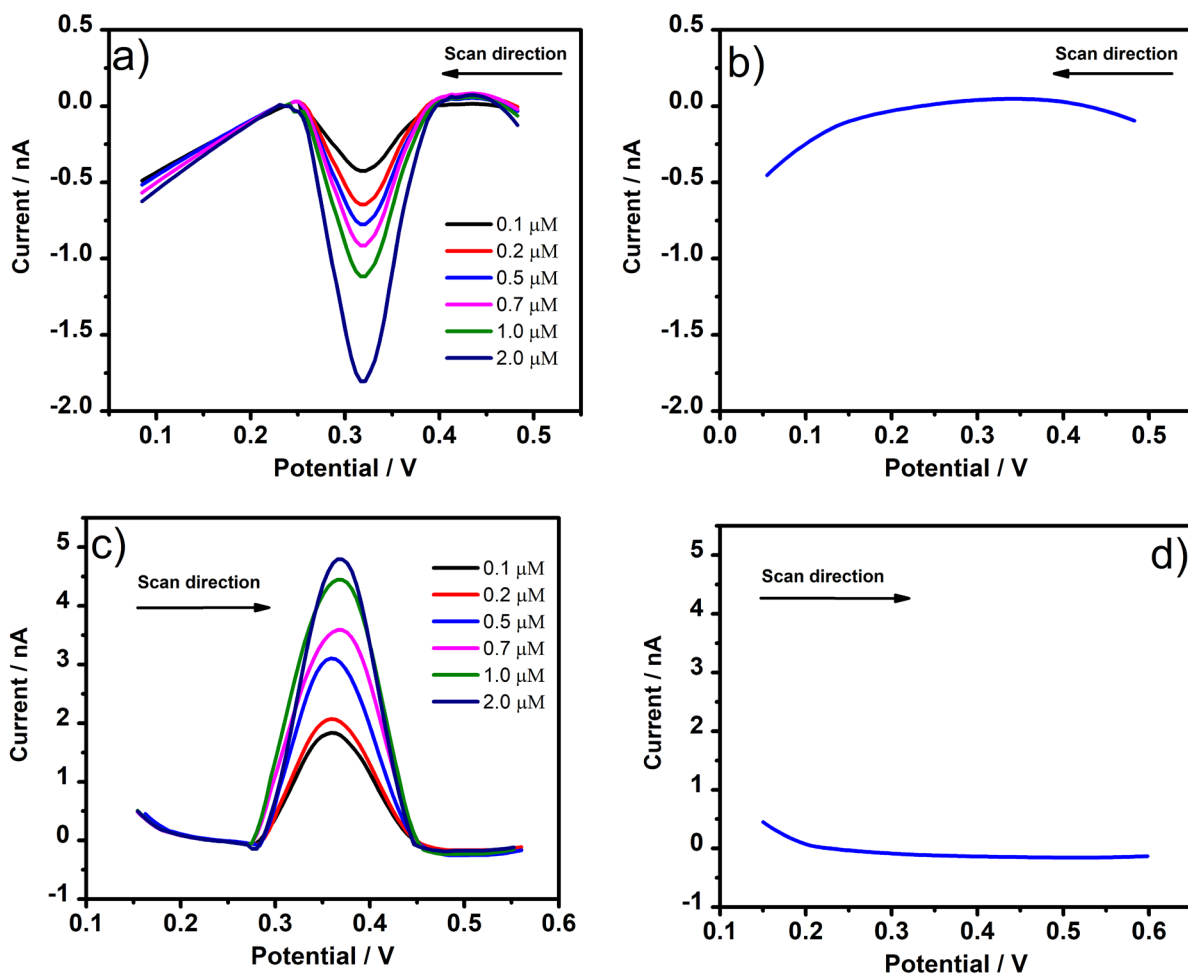


**Figure S2.** Differential pulse voltammetry (DPV) of increasing PFOS<sup>-</sup> concentrations at the  $\mu$ ITIES array for (a) forward scan and (b) corresponding background forward scan. DPV of increasing PFOS<sup>-</sup> concentrations at the  $\mu$ ITIES array for (c) reverse scan and (d) corresponding background reverse scan. Aqueous phase: 10 mM LiCl. Organic phase: 10 mM BTTPATPBCl.

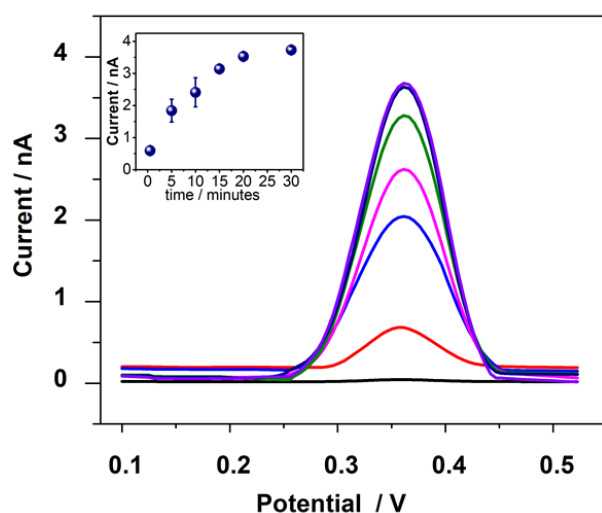
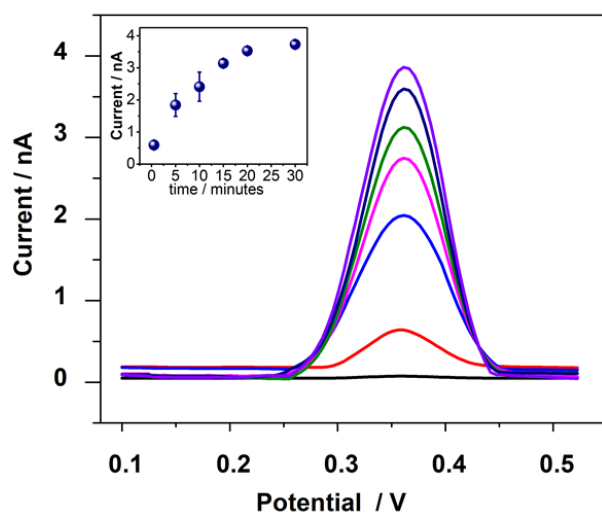


**Figure S3.** Additional data sets for the influence of the preconcentration time on the DPSV (background-subtracted) of 10 nM PFOS<sup>-</sup> at the  $\mu$ ITIES array. Preconcentration times: 0.0 (black line), 0.5, 5, 10, 15, 20, 30 min. These data are repetitions of the data shown in Fig. 3. Inset: plot of stripping peak current versus preconcentration time, noting that the data point for 0.0 min preconcentration time is not shown in the inset graph. Data points are averages of three measurements and error bars are  $\pm 1$  standard deviation. Where error bars are not visible, they are smaller than the symbol size. Note that the inset plots here and in Figure 3 are identical – they all show the same average ( $\pm$  standard deviation) data.

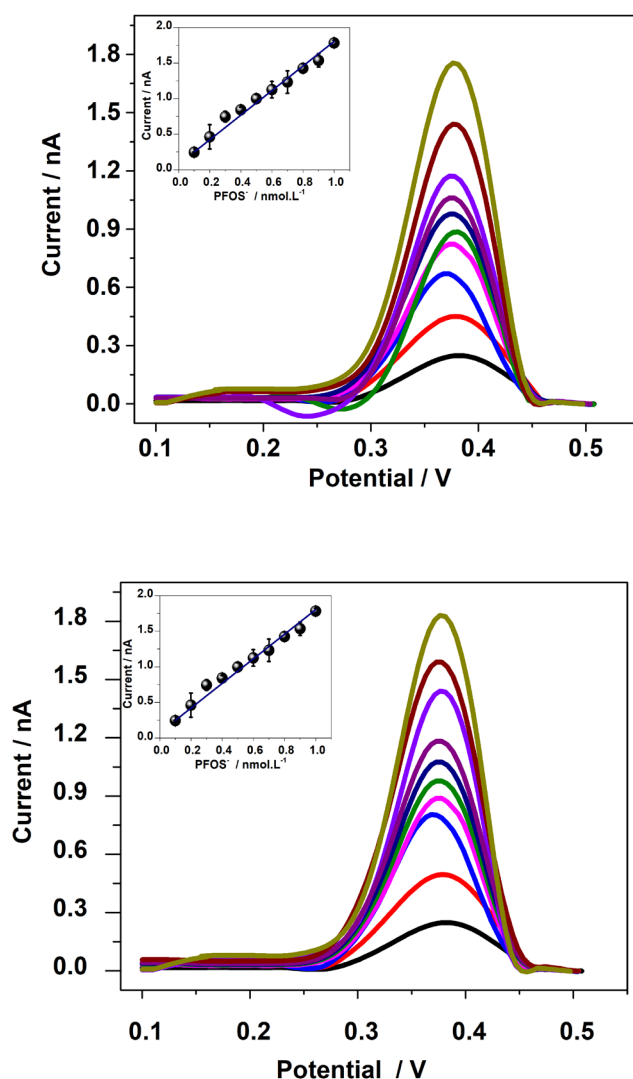


**Figure S4.** Additional data sets for electrochemistry of increasing concentrations of PFOS<sup>-</sup> at the  $\mu$ TIES array using DPSV (background subtracted). Concentration range 0.1 to 1.0 nM PFOS<sup>-</sup>. These data are repetitions of the data shown in Figure 4. Inset: calibration curve of current versus concentration. Data points are averages of three measurements and error bars are  $\pm 1$  standard deviation. Where error bars are not visible, they are smaller than the symbol size. Note that the inset plots here and in Figure 3 are identical – they all show the same average ( $\pm$  standard deviation) data.

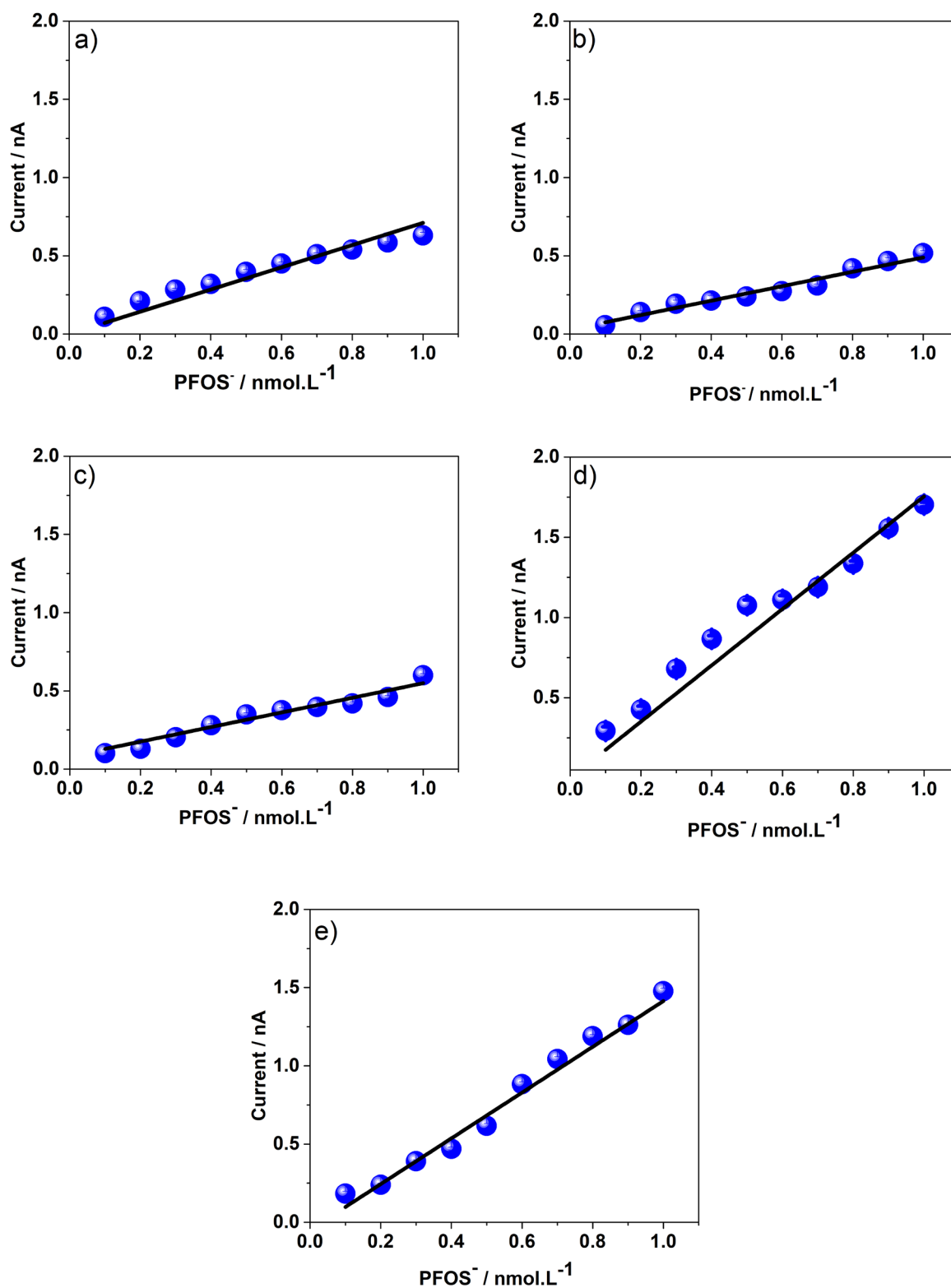


**Figure S5.** Calibration curve of DPSV stripping peak current versus concentration a) Drinking water + 10 mM LiCl, b) Laboratory tap water + 10 mM LiCl, c) Drinking water without LiCl, d) Seawater + 10 mM LiCl, e) Seawater without LiCl.